García-Rodríguez, Luis Fernando; Chacón Velasco, Jorge Luis

Chicamocha canyon wind energy potential and VAWT airfoil selection through CFD modeling

Chicamocha canyon wind energy potential and VAWT airfoil selection through CFD modeling

Energía eólica del Cañón del Chicamocha y selección del perfil aerodinámico para una VAWT usando CFD

Luis Fernando García-Rodríguez [ID]1*, Julian E. Jaramillo [ID]1, Jorge Luis Chacón Velasco [ID]1

1Departamento de Ingeniería Mecánica, Universidad Industrial de Santander UIS. Cra. 27 calle 9. C.P. 680002. Bucaramanga, Colombia.

ABSTRACT: The use of vertical axis wind turbines (VAWT) in Colombia could tackle the energy distribution difficulties as large parts of the territory are not connected to the electrical grid. The present research experimentally determines the wind resource available of a rural place known as Chicamocha's canyon and selects the airfoil for a VAWT blade through CFD modeling. By using the mean wind speed of the location, the performance of the NACA0018 and DU06W200 airfoils is evaluated in terms of the lift and drag coefficients through a 2D CFD modeling using OpenFOAM and the "Spalart-Allmaras fv3" turbulence model. It is found feasible the use of wind energy at the location where the mean year density power is **485 [W/m^2]**, and the DU06W200 airfoil is suggested for constructing the blades of a VAWT, as its aerodynamic efficiency (c_l/c_d) overcomes by 14% the commonly used NACA0018.

RESUMEN: El uso de turbinas eólicas de eje vertical (VAWT) en Colombia podría abordar las dificultades de distribución de energía ya que gran extensión del territorio no está conectado a la red eléctrica. La presente investigación determina experimentalmente la potencia eólica disponible en el sector rural conocido como "Cañón del Chicamocha" y selecciona el perfil aerodinámico para diseñar un aspa de una VAWT por medio de simulación 2D en CFD. Tomando las características del viento del sitio de interés, se determina el desempeño aerodinámico de los perfiles NACA0018 y DU06W200 mediante el cálculo de sus coeficientes de sustentación y arrastre usando OpenFOAM considerando el modelo de turbulencia "Spalart-Allmaras fv3". Esta investigación muestra viable el uso de la energía eólica en el Cañón del Chicamocha al determinar la potencia eólica promedio anual de **485 [w/m^2]**, además, sugiere construir los álabes de la turbina eólica usando el perfil aerodinámico DU06W200 al ser 14% más eficiente que el comercialmente usado NACA0018.

1. Introduction

According to the Mining and Energy Planning Unit of Colombia (UPME) [1], 52% of Colombian territory is not connected to the local grid and the energy demand is going to duplicate in the next 40 years. Furthermore, 75% of the energy is supplied by hydroelectric power that could have a negative impact on the environment [1]. Nowadays, there is only one wind farm that produces 19.5 MW in the country [1], but the wind direction changes constantly due

to Colombian topography. So, there is a need of developing wind power solutions capable of using this fluctuating resource in order to diversify the energy portfolio. This research is the first one in analyzing the wind power density at the Chicamocha's canyon, the second largest canyon worldwide, which needs to improve its surroundings infrastructure to promote tourism [2]. The electrical grid at the canyon is not stable due to its topography, and local community need a sustainable source of energy that does not impact the environment, and ensures an economic growth in the tourism industry. Therefore, one of the main purposes of this research is to determine the feasibility for installing Vertical Axis Wind Turbines (VAWT) there.

The performance of a VAWT relies principally on its airfoil, which generates lift and drag forces that take advantage of the wind kinetic energy to produce torque at the shaft of the turbine. Airfoil design and selection is an important task that depends on three main topics: wind flow conditions, airfoil shape, and modeling. Currently, Darrieus VAWT blades design are based on lift aerodynamic force and uses the commercial NACA0018 airfoil. A previous research [3] developed a new airfoil for these turbines: the DU06W200 airfoil, which overcomes the aerodynamic performance of the NACA0018. In that work, experiments and modeling of the airfoil based on Blade Element Momentum (BEM) theory are proposed. Nevertheless, the Reynolds numbers analyzed are higher than those observed in the Chicamocha's Canyon. Furthermore, the drag coefficient calculated through their developed software, RFOIL, overestimates the experimental values. Then [4] compared the airfoils DU06W200 and NACA0021 in terms of energy performance and aerodynamic forces. The analysis is done with the commercial Computational Fluid Dynamics (CFD) software "Fluent 6.3.26" for a $Re = 5.3 \times 10^4$ applying the "k-ε Realizable" [5] turbulence model. However, a validation of the turbulence model is not presented, the pressure coefficient distribution is not conclusive and nor lift or drag values are presented. The NACA0018 airfoil has been studied previously too for wind turbines, e.g. [6] analyzed that airfoil performance for horizontal wind turbines at the wind speed of 32 [m/s], but the application differs from the one this research is looking. Also experimental tests were conducted such as [7] focused on transition over the NACA0018 airfoil at a Reynolds number of 1×10^5 and analyzed the shear layer distribution. Other CFD simulations of the NACA0018 airfoil are available such as [8–10], however the Reynolds numbers analyzed are not in the range of Chicamocha's canyon needs. The [11] research meet the requirements of the current research but only one angle of attack is analyzed. Therefore, this research complements the previous studies by increasing the range of Reynolds numbers analyzed for the DU06W200 airfoil, providing further information about the aerodynamic global coefficients and analyzing the performance of both airfoils under different attack angles.

This work has a double purpose. First, determining the feasibility installation of VAWT at Chicamocha's canyon. Second, selecting the airfoil for the wind turbine blade that presents highest aerodynamic efficiency under the wind flow conditions found at Chicamocha's canyon. The present study applies a CFD numerical approach by means of the free software "OpenFOAM". Turbulence is solved by the one equation RANS model developed by Spalart-Allmaras [12]. The geometry of the airfoils studied, i.e. DU06W200 and NACA0018, can be seen in Figure 1.
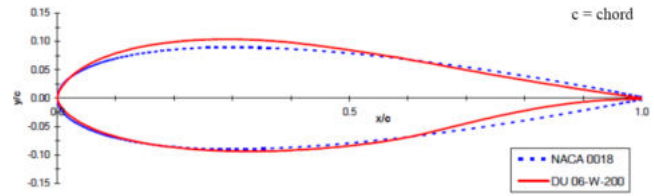

Figure 1 Comparison between airfoils NACA0018 and DU06W200 [3]

2. Methodology

Figure 2 shows the research scheme applied in this study. The work is composed by two components: firstly, a wind density potential study of Chicamocha's canyon, and secondly, a CFD modeling aimed to compare the airfoil's performance under realistic conditions to suggest one for the wind turbine blades.

2.1 Installation feasibility of VAWT´s at Chicamocha's canyon

The Chicamocha's canyon national park, known as "PANACHI", monitor constantly the wind velocity at the canyon to control the cableway safety installed at the location. The administration of the park provided to this research the historical of the data from the year 2009 up to 2012. It possesses the wind velocity magnitude at the places known as "Mesa de los Santos", "Chicamocha's River" and "PANACHI" (Figure 3). The historical includes daily information at three schedules: 8:00 am, 12:00 pm and 5:00 pm.

By using the collected data, the feasibility of installing a VAWT is analyzed. The mentioned wind turbines are suggested for the location since the blades do not need to be pointed towards the wind direction to be effective. Moreover, its structural and aesthetic principles have improved power generation in turbulent flows [4, 14].

The wind energy potential of the canyon is analyzed by using the mass conservation principle (Equation 1):

$$\frac{dm}{dt} = \rho * A * U \qquad (1)$$

where ρ is the air density, U the velocity and A is the swept area. Then, the wind energy potential, P, can be expressed as kinetic energy per time unit as (Equation 2):

$$\frac{P}{A} = \frac{1}{2} * \rho * U^3 \qquad (2)$$

In this research the criterion presented in [14] is taken into account to establish how significant the wind energy potential is at a selected location (Table 1).
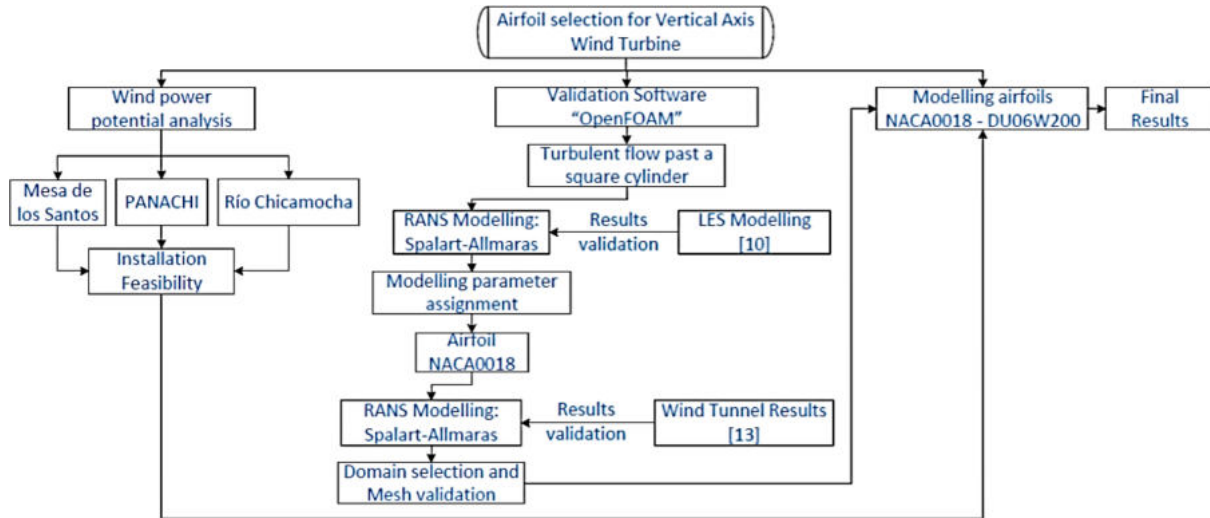
Figure 3 Satellite view of the wind measurements sites at Chicamocha canyon [13]

Table 1 Wind power potential criterion [14]

$P/A < 100 \ W/m^2$	Poor
$P/A \approx 400 \ W/m^2$	Good
$P/A > 700 \ W/m^2$	Excellent

2.2 Aerodynamic study

The wind flow incidence over the airfoil generates a force distribution along its surface, which can be decomposed into lift and drag force (Figure 4).
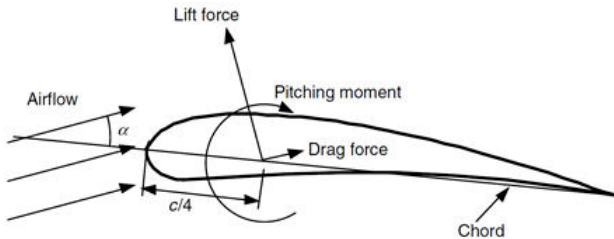

Figure 4 Forces and momentum over an airfoil, α angle of attack, c chord length [14]

These parameters are defined through their dimensionless coefficients: Lift coefficient, c_l, and drag coefficient, c_d, defined in Equation 3 and 4 respectively.

$$C_l = \frac{L/l}{\frac{1}{2}\rho U^2 c} \tag{3}$$

$$C_d = \frac{D/l}{\frac{1}{2}\rho U^2 c} \tag{4}$$

Where L/l and D/l indicate the lift and drag force per unit span of the wing respectively, and c the airfoil's chord. By using the Dynamic Similitude concept [14] the airfoil's performance depends on the attack angle, the Mach and the Reynolds numbers.

2.3 CFD airfoil studies

Different researchers have improved airfoil's performance for wind turbines by means of wind tunnel tests and theoretical studies [1, 11]. Nevertheless, these efforts are time-consuming and need high technology laboratories [14]. Therefore, the use of simulation tools has become crucial to develop a wide range of aerodynamic technologies. For fluids, the CFD use has increased in the past decades since the modeling of the flow allows the analysis of microscopic scales that cannot be easily captured in experimental tests.

The incompressible fluid flows are governed by the Navier Stokes equations of mass conservation (Equation 5) and momentum (Equation 6).

$$\frac{\partial \rho}{\partial t} + \nabla \cdot (\rho u) = 0 \tag{5}$$

$$\frac{\partial}{\partial t}[\rho u] + \nabla \cdot (\rho u u) = -\nabla p + \nabla \cdot \{\mu[\nabla u + (\nabla u)^T]\} + \boldsymbol{f}_b \tag{6}$$

These equations are nonlinear and can be handled by adopting an iterative approach. Nevertheless, there is none explicit equation for computing the pressure field that appears in the momentum equation. Moreover, solving general fluid flows requires an algorithm that can deal with the pressure-velocity gradient coupling.

In the present research the flow is assumed to be steady, turbulent and incompressible, therefore the continuity and momentum equations (written in conservative form) are expressed in Equations 7 and 8.

$$\triangledown \cdot u = 0 \tag{7}$$

$$\rho\left(\triangledown u\right)u = -\triangledown p + \mu \triangledown \cdot \left(\triangledown u + \left(\triangledown u\right)^T\right) \tag{8}$$

The turbulence regime can be solved either Direct Numerical Simulation (DNS) or Indirect Numerical Simulation (INS). The DNS solves each temporal and spatial fluctuation scale of the vortex energy cascade, but the computational cost is large enough to make it unfeasible for solving industrial applications due to the high-density meshing and short temporal steps needed [15]. On the other hand, an INS applies either a temporal averaging (RANS) or a spatial average fluctuation, to model the vortex generation and uses a turbulence model to close the system of equations. That make INS feasible for industrial applications as the current research requirements. A RANS filtering is applied to the governing equations of the flow leading to Equations 9 and 10.

$$\frac{\partial \overline{u}_i}{\partial x_i} = 0 \tag{9}$$

$$\rho\frac{\partial \overline{u}_i\overline{u}_j}{\partial x_j} = -\frac{\partial \overline{p}}{\partial x_i} + \frac{\partial}{\partial x_j}\left(\mu\frac{\partial \overline{u}_i}{\partial x_j} - \rho\overline{u'_i u'_j}\right) \tag{10}$$

The term $\rho\overline{u'_i u'_j}$ is the Reynolds stress tensor and represents correlations between fluctuating velocities. In order to model it, the Spalart Allmaras-fv3 (S-A fv3) turbulence model is selected due to literature recommendations [16] and a turbulence model validation described in Section 3 . The model is described as follows (Equation 11 - 21):

$$\overline{-u'_i u'_j} = 2v_t S_{ij} \tag{11}$$

$$\begin{aligned}\frac{\partial \hat{v}}{\partial t} + u_j\frac{\partial \hat{v}}{\partial x_j} &= c_{b1}\left(1 - f_{t2}\right)\hat{S}\hat{v} \\ &- \left[c_{w1}f_w - \frac{c_{b1}}{k^2}f_{t2}\right]\left(\frac{\hat{v}}{d}\right)^2 \\ &+ \frac{1}{\sigma}\left[\frac{\partial}{\partial x_j}\left((v + \hat{v})\frac{\partial \hat{v}}{\partial x_j}\right) + c_{b2}\frac{\partial \hat{v}}{\partial x_i}\frac{\partial \hat{v}}{\partial x_i}\right]\end{aligned} \tag{12}$$

$$v_t = \mu_t/\rho \iff \mu_t = \rho\hat{v}f_{v1} \tag{13}$$

$$f_{v1} = \frac{X^3}{X^3 + c_{v1}^3} \tag{14}$$

$$X = \frac{\hat{v}}{v} \tag{15}$$

$$\hat{S} = f_{v3}\Omega + \frac{\hat{v}}{k^2d^2}f_{v2} \tag{16}$$

where $\Omega = \sqrt{2W_{ij}W_{ij}}$ is the vorticity magnitude and d the distance to the nearest wall. Finally, is given:

$$f_{v2} = 1 - \frac{X}{\left(1 + X/c_{v2}\right)^3}; \; f_w = g\left[\frac{1 + c_{w3}^6}{g^6 + c_{w3}^6}\right]^{\frac{1}{6}} \tag{17}$$

$$g = r + c_{w2}\left(r^6 - r\right); r = min\left[\frac{\hat{v}}{\hat{S}k^2d^2}, 10\right] \tag{18}$$

$$f_{t2} = c_{t3}\text{exp}\left(-c_{t4}X^2\right); W_{ij} = \frac{1}{2}\left(\frac{\partial v_i}{\partial x_j} - \frac{\partial v_j}{\partial x_i}\right) \tag{19}$$

$$f_{v3} = \frac{\left(1 + xf_{v1}\right)\left(1 - f_{v2}\right)}{x} \tag{20}$$

$$c_{v2} = 5 \tag{21}$$

By using the Finite Volume Method (FVM), the partial differential equations representing conservation laws (Equations 9 and 10) are transformed into discrete algebraic equations. The FVM is a conservative method as the flux entering into a given volume is identical to the outflow of the adjacent volume. In addition, it can be formulated at unstructured polygonal meshes as the unknown variables are evaluated at the centroids of the volumes and not at their faces. The method starts with the discretization of the geometric domain, i.e. divide the domain into non-overlapping finite volumes. Then, the partial differential equations are discretized into algebraic equations by its integration over each discrete volume. Finally, the system of algebraic equations is solved to compute the dependent variable at each of the control volumes. By using this FVM method, some terms in the conservation equation are turned into fluxes evaluated at the faces of the finite volumes. The discretized form of the momentum and mass conservation equations can be seen at Equations 22 and 23.

$$\Sigma_{f\sim nb(C)}\dot{m}_f = \dot{m}_e + \dot{m}_w = 0 \tag{22}$$

$$\begin{aligned}a_e u_e^* &= \sum a_{nb}u_{nb}^* + b + \left(p_p^* - p_E^*\right)A_e \\ a_n v_n^* &= \sum a_{nb}v_{nb}^* + b + \left(p_p^* - p_N^*\right)A_n \\ a_t w_t^* &= \sum a_{nb}w_{nb}^* + b + \left(p_p^* - p_T^*\right)A_t\end{aligned} \tag{23}$$

Equation 23 can be solved only when the pressure field is given or estimated. Unless the correct pressure field is employed, the resulting velocity field will not satisfy the

relation. Therefore, an initial velocity field (u^*, v^*, w^*) is calculated based on a guessed pressure distribution (p^*) to start the iterations. Then, a new value of pressure (p) is updated from Equation 24.

$$p = p^* + p' \tag{24}$$

where p' is described at Equation 25.

$$a_{c,c}p'_{c,c} = a_{E,c}p'_{E,c} + a_{W,c}p'_{W,c} + a_{c,N}p'_{c,N} + a_{c,s}p'_{c,S} + b'_{c,c}$$
$$a_{c,c} = a_{E,c} + a_{W,c} + a_{c,N} + a_{c,S}$$
$$a_{E,c} = (\rho dA)_{e,c}$$
$$a_{W,c} = (\rho dA)_{w,c}$$
$$a_{c,S} = (\rho dA)_{c,s}$$
$$b'_{I,J} = (\rho u^* A)_{w,c} - (\rho u^* A)_{e,c} + (\rho v^* A)_{c,s} - (\rho u^* A)_{c,n} \tag{25}$$

Once the pressure is updated, the velocity is corrected with Equations 26 - 28.

$$u_e = u_e{}^* + d_e\left(p_{P}{}' - p_{E}{}'\right) \tag{26}$$

$$v_n = v_n{}^* + d_n\left(p_{P}{}' - p_{N}{}'\right) \tag{27}$$

$$w_t = w_t{}^* + d_t\left(p_{P}{}' - p_{T}{}'\right) \tag{28}$$

The described process corresponds to the Semi-Implicit Method for Pressure-Linked (SIMPLE) algorithm, which can be summarized as [16]:

a) Guess the pressure field p^*.

b) Solve Equation 23 to obtain u^*, v^*, w^*.

c) Solve the p' using Equation 25.

d) Calculate p by adding p' to p^*.

e) Calculate u, v, w from their started values using Equations 26-28.

f) Solve the discretization equation for other $\phi's$ (such as temperature, concentration, and turbulent quantities) if they influence the flow field through fluid properties, source terms, etc.

g) Treat the corrected pressure p as a new guessed pressure p^*, return to step b) and repeat the whole pressure until convergence is reached.

2.4 OpenFOAM modeling description

Different tests are made and compared with the literature to verify the mathematical models used. The type of boundaries established can be seen in Table 2.

The numerical schemes are shown in Table 3. The boundary conditions and initial values of the variables are described in Table 4. Finally, the equations solvers, tolerances, and algorithms are shown in Table 5.

3. Discussion and analysis of results

3.1 "Mesa de los Santos" wind speed measuring

The annual average wind speed range from 5 up to 7 [m/s], giving a maximum wind power density of $450[W/m^2]$ on February and minimum of 180 $[W/m^2]$ on July (Figure 5).
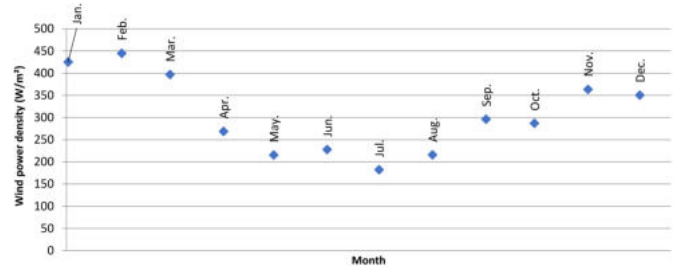

Figure 5 Monthly wind power density at "Mesa de los Santos"

3.2 Chicamocha's river wind speed measuring

At this location, wind flow accelerates due to mountains that surround the river, which acts as a nozzle directing the wind to a smaller section (Figure 6).
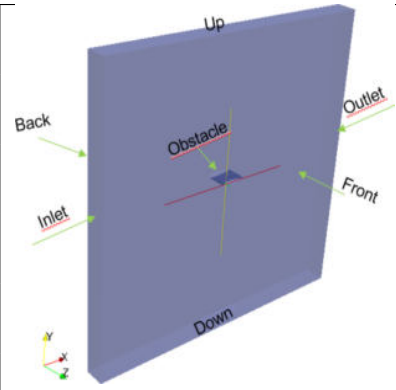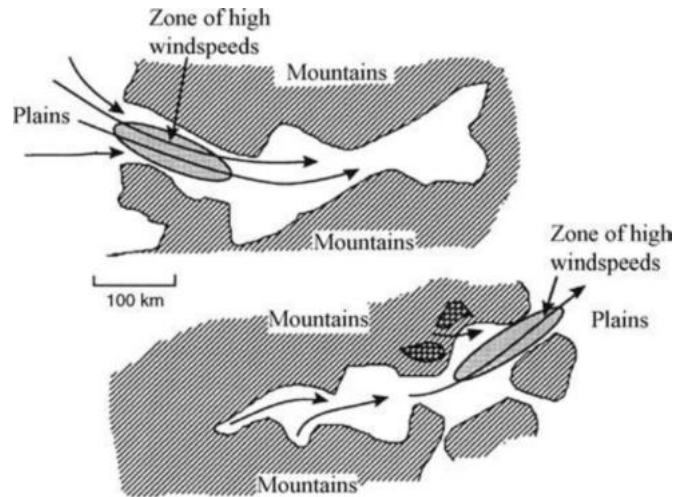

Figure 6 Wind speed increase due to canalization of prevailing winds from the mountain. [14]

This effect is confirmed by the wind speed measured at the location, with peak value of 8.8 [m/s] and peak wind power density of $770[W/m^2]$ as Figure 7 shows.

Table 2 Patches used at the airfoil domain [Author]

Patch	Type
Inlet	Patch
Outlet	Patch
Front and Back	Empty (2D modeling)
Obstacle	Wall
Up and down	Patch

Table 3 Numerical time schemes used [Author]

Mathematical term	OpenFOAM keyword	Used
Cell to face interpolations of values	interpolationSchemes	*Lineal* (central differences)
Component of gradient normal to a cell face	snGradSchemes	*Corrected:* does not required an explicit correction of the non-orthogonally.
Gradient ∇	gradSchemes	*Gauss:* standard discretization of the finite volumes by the Gaussian integral.
Divergence $\nabla\cdot$	divSchemes	(*phi, U*) bounded Gauss (*phi, nuTilda*) linearUpwind (*nuEff*) Gauss linear
Laplacian ∇^2	laplacianSchemes	Gauss Linear corrected
First and second time derivatives, e.g. $\frac{\partial}{\partial t}, \frac{\partial^2}{\partial t^2}$	timeScheme	steadyState

Table 4 Boundary conditions at the Patches [Author]

Boundary	v_t	$\hat{v}$	p	u[m/s]
Inlet	$v_t = 0.02221$	$\hat{v} = 0.0221$	$\frac{\partial p}{\partial n} = 0$	$u = 18$
Outlet	$v_t = 0.02221$	$\hat{v} = 0.0221$	$p = 0$	$\frac{\partial u}{\partial n} = 0$
obstacle	nutUSpaldingWallFunction y^+ $= u^+$ $+\frac{1}{E}\left[\exp\left(ku^+\right) - 1 - ku^+\right.$ $\left. -0.5\left(ku^+\right)^2 - \frac{1}{6}\left(ku^+\right)^3\right]$	nutUSpaldingWallFunction y^+ $= u^+$ $+\frac{1}{E}\left[\exp\left(ku^+\right) - 1 - ku^+\right.$ $\left. -0.5\left(ku^+\right)^2 - \frac{1}{6}\left(ku^+\right)^3\right]$	$\frac{\partial p}{\partial n} = 0$	$u = 0$
Front and Back	empty			
Up and Down	$v_t = 0.0221$	$\hat{v} = 0.0221$	$\frac{\partial p}{\partial n} = 0$	$u = 18$

3.3 National park of Chicamocha (PANACHI) measurement

The maximum wind speed value is found in January with a value of 5.7 [m/s] and wind power density of 180 *[W/m²]*. Figure 8 shows the results.

Table 6 summarizes the annual average wind speed and wind power density of the three locations. In brief, the feasible place for VAWT locations is at Chicamocha's river due to its high average wind speed, 6.9 [m/s].
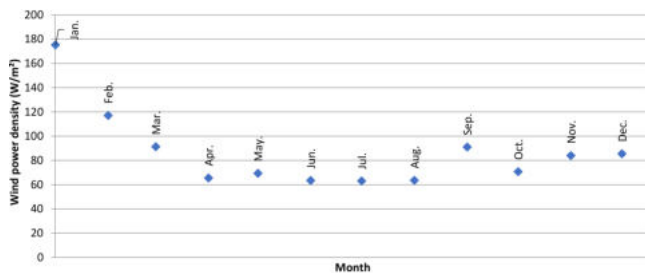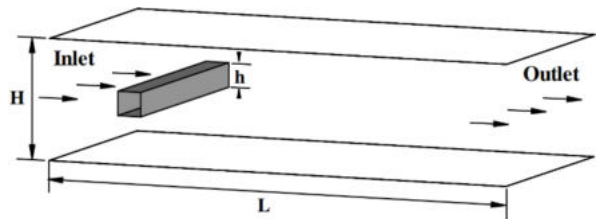
3.4 Validation and verification

Table 5 Numerical time schemes used [Author]

Description	OpenFOAM keyWord	Used	
Linear Solver Control	solver	p	GAMG
		U $nuTilda$	smoothSolver
	smoother	GaussSeidel	
	tolerance	p	1e-6
		U $nuTilda$	1e-8
Algorithm	-	SIMPLE	
Controls under-relaxation	relaxationFactors	p	0.3
		U $nuTilda$	0.7

Table 6 Wind power potential at Chicamocha's canyon [Author]

Place	Annual average wind speed [m/s]	Standard deviation	Annual average wind power density [W/m^2]
"Mesa de los santos"	5.9	0.736	306.188
Chicamocha's River	6.9	1.084	485.115
"PANACHI"	4.3	0.536	86.643
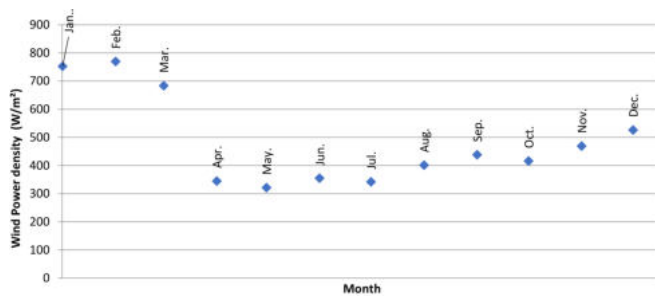
Figure 7 Monthly wind power density at Chicamocha's river

Figure 9 Physical Configuration [17]

Figure 8 Monthly wind power density at PANACHI

Comparison between RANS and LES of turbulent flow past a square cylinder confined in a Channel

A square cylinder confined in a channel is simulated using different turbulence models to select the one that most approaches to literature results [17]. The influence of the mathematical simplifications and the SIMPLE algorithm is also analyzed. The domain used is shown in Figure 9.

The fluid properties are incompressible flow, Re: 3×10^3, steady state, 2D and blockage ratio of 20%. A uniform velocity profile with a thin boundary layer thickness of 6% of channel height is necessary to replicate the case [17]. The boundary conditions used are the same as Table 4, modifying the initial values of the variables according to the fluid properties mentioned.

A Cartesian orthogonal mesh is used and refined at the boundaries of the obstacle, i.e. cube, as Figure 10 shows. Velocity components and turbulent fluctuations are averaged in time and in the cross-stream direction.

At Figure 11, the mean streamwise velocity along the centerline is shown for different simulations varying the mesh density. The results are compared with the literature [17] (black line). This comparison is performed to find the mesh independence, which is at 5×10^5 cells, giving an average difference around 12% and standard deviation of 0,283. Therefore, the "simpleFoam" algorithm is validated for the Spalart-Allmaras fv3 turbulence model.
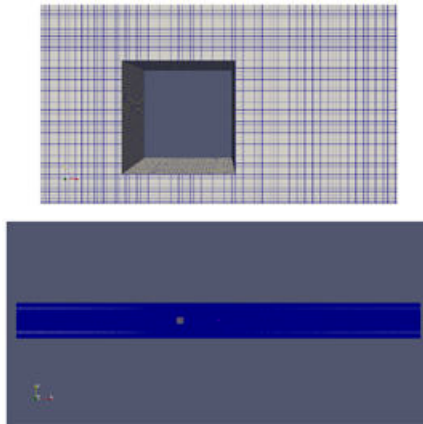
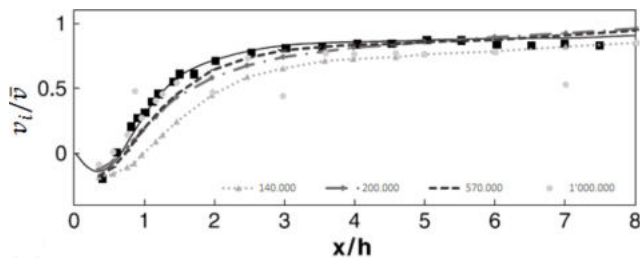Figure 10 Structured quadrangular mesh used [Author]

Figure 11 Mesh independence: Mean streamwise velocity profile along the centerline (■ and black line - literature [17]

By using the same modeling conditions and a mesh distribution of $5x10^5$ volumes, different turbulence models were analyzed: k-W SST, k-E Launder-Sharma and Spalart-Allmaras fv3. The results shown at Figure 12, concludes that Spalart-Allmaras fv3 model keeps the most accurate distribution in comparison with literature.
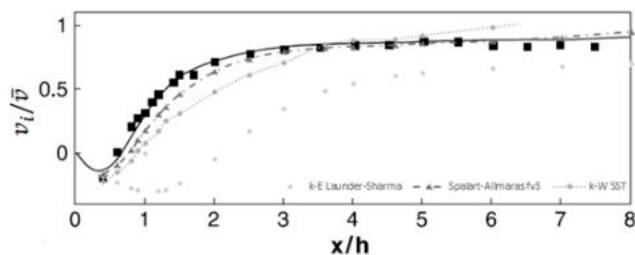

Figure 12 Turbulence models comparison: Mean streamwise velocity profile along the centerline (black line: literature [17])

DU06W200 modeling comparison between simpleFOAM and RFOIL software

The RFOIL software used in [3] based on BEM theory is compared with the current CFD results for Re $= 5 \times 10^5$, $\alpha = 0^o$, c $= 0.25$[m] and free transition. To ensure a develop flow that reaches the airfoil, a channel length of 36c upwind, 44c downwind and a blockage ratio of 20% is
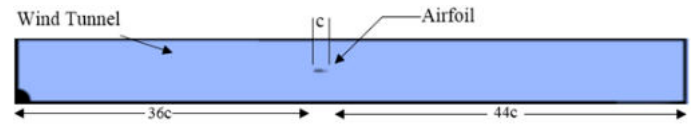
designed (Figure 13).

Figure 13 Wind tunnel measurements. [Author]

A Cartesian orthogonal mesh is used and refined at the boundaries of the airfoil (Figure 14). In addition, different meshes densities are analyzed for the Spalart-Allmaras fv3 turbulence model (Figure 15).

The Figure 15 shows no significant variation after the mesh density of 3.6×10^5 volumes. The CFD results follow the pressure distribution showed by the RFOIL software with an average difference of 15%. At high Reynolds numbers, RFOIL has problems to predict airfoil characteristics, e.g. it overestimates the maximum lift coefficient [3]. Such variation might be presented due to the lack of accuracy found at the trailing edge of the airfoil, where the turbulence model is sensible to vortex variations. Therefore, the CFD simulations will be used as the reference model.

NACA0018 validation with experimental tests

The numerical results are validated by comparing the lift and drag coefficients from the literature [7]. The airfoil is simulated under three different angles of attack: 0º, 10º, and 20º. The chord length (c) of the airfoil is 0.25 [m] and a Reynolds number of 3×10^5. Results are shown in Table 7, Table 8 and Table 9. The boundary conditions are the same mentioned at Table 4. The 'nutUSpaldingWallFunction" provides a turbulent kinematic viscosity condition when using wall functions for rough walls, based on velocity, using Spalding's law to give a continuous nut profile to the wall ($y+ = 0$).

Table 7 y^+ Results for different angles of attack [Author]

α	y + $_{min}$	y + $_{max}$	y + $_{mean}$
0º	1.614	15.979	10.775
10º	0.636	16.436	9.58
20º	0.922	18.456	8.222

Table 8 Lift coefficients of the airfoil NACA0018 at different angles of attack [Author]

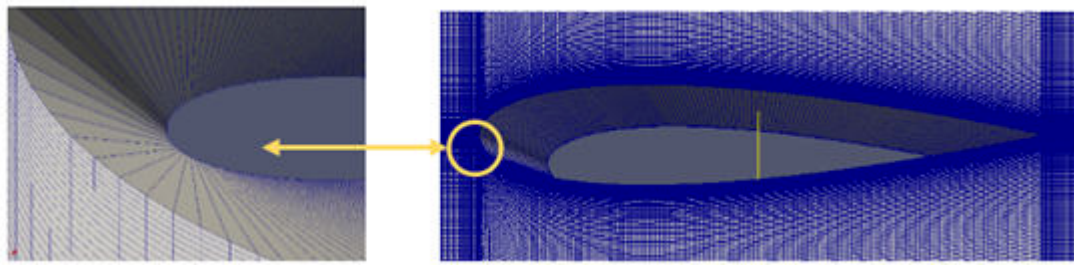| α	Cl $_{simulacion}$	Cl $_{túnel}$	% Difference
0º	0.0204	0.0193	5.7
10º	0.664	0.803	17.31
20º	0.769	0.615	25

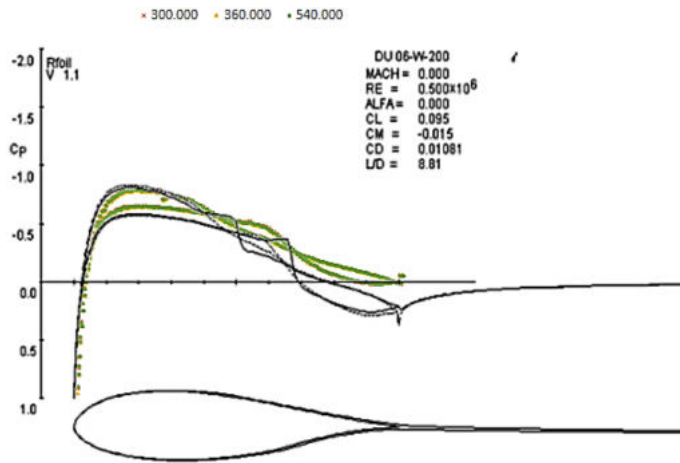**Figure 14** Mesh detail around NACA0018 airfoil

Figure 15 DU06W200 RFOIL and CFD data for $Re = 5 \times 10^5$ and $\alpha = 0^o$ (black line: literature [3], color lines: present)

**Table 9** Drag coefficients of the airfoil NACA0018 at different angles of attack [Author]

α	$Cd_{simulación}$	$Cd_{túnel}$	% Difference
0°	0.0379	0.0324	16.97
10°	0.0646	0.059	9.49
20°	0.206	0.243	15.22

Wind flow behavior of the airfoil NACA0018 is shown in Figure 16.

The implemented turbulence model accuracy is acceptable, presenting a maximum variation of 17% in comparison to the wind tunnel tests [7]. The higher performance of the airfoil is found at the attack angle of 10°, where the lift and drag coefficients ratio has the greatest value: 10.3 approximately. Figure 16 shows a greater acceleration of the flow produced around the airfoil for an angle of attack of 0°, but as the angle of attack increases, the flow separation moves towards to the leading edge at the upper surface. It produces large vortex perceivable at the angle of attack of 20° at the trailing edge, which results in higher drag.
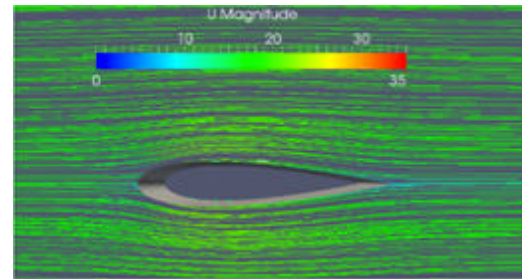
(a)
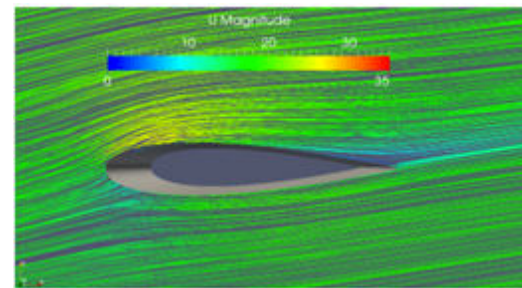
(b)
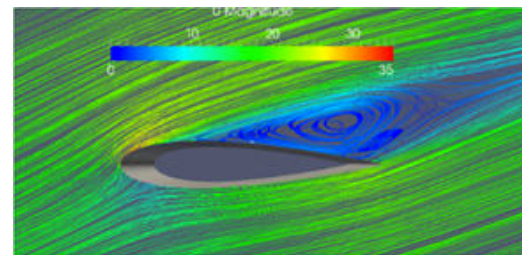
(c)

Figure 16 Wind velocity vectors over the airfoil at different angles of attack: (a) 0°, (b) 10° and (c) 20° [Author]

3.5 Results

Airfoils NACA0018 and DU06W200: performance analysis for Reynolds numbers between 2 x 10⁵ and 3.4 x 10⁵

This part analyzes the Reynolds number influence on the global aerodynamic parameters of each airfoil by using the FVM under the Spalart-Allmaras fv3 turbulence model. Similar grid size is adapted to each airfoil for this study.

Table 10 Wind properties established to compare the NACA0018 and DU06W200 airfoil's performance

	Re 2×10^5	Re 3×10^5	Re 3.4×10^5
Wind Speed [m/s]	7.5	18	20
$\tilde{v} = 3v_\infty$	0.107	0.276	0.306
$v_t = \sqrt{1.5}u_\infty Il$	0.0107	0.0276	0.0306

The modeling conditions are $\alpha = 10^o$, $c = 0.25[m]$ and the fluid properties mentioned in Table 10. Where $\tilde{v}$ is the modified turbulent viscosity and v is the turbulent viscosity. The drag and lift coefficients are used in order to analyze the performance of the airfoils. The values can be seen at Table 11.

Table 11 Lift and drag coefficients from the airfoils NACA0018 and DU06W200 under different Reynolds numbers [Author]

Reynolds Number	NACA0018		DU06W200	
	Cd	Cl	Cd	Cl
2×10^5	0.08	0.707	0.085	0.876
3×10^5	0.065	0.664	0.075	0.884
3.4×10^5	0.07	0.687	0.077	0.926

It can be concluded under the same Reynolds number, the lift coefficient of the DU06W200 airfoil overcomes in 23.3% the one from the NACA0018. As the Reynolds number increases, the lift coefficient increases too and the performance of the DU06W200 corresponds to the expectations of [3] design.

3.6 Airfoils modeling under Chicamocha's canyon wind speed

**Table 12** Lift and drag coefficients of the airfoils NACA0018 and DU06W200 under Chicamocha's canyon wind speed [Author]

AIRFOIL	Cl	Cd
NACA0018	0.707	0.0801
DU06W200	0.876	0.0853

The wind speed is the highest found at the analyzed locations, i.e. Chicamocha's river ($u = 6.93$ [m/s]). The chord length of the airfoil, Reynolds number and angle of attack are defined at following: c = 0.25 [m], $Re = 1.19 \times 10^5$, steady-state regime and $\alpha = 10^o$.
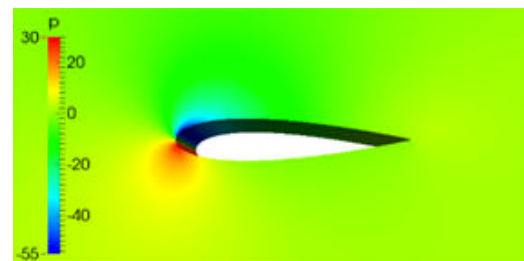
Figure 17 shows that wind speed at the leading edge of the airfoil DU06W200 is greater than NACA0018, confirming the airfoil optimization developed by [3]. Therefore, the cambered airfoil DU06W200 generates a high-pressure peak followed by a sharp fall of its values, as Figure 18 shows.
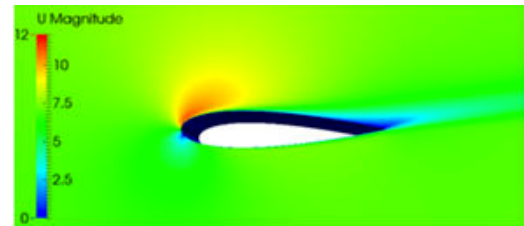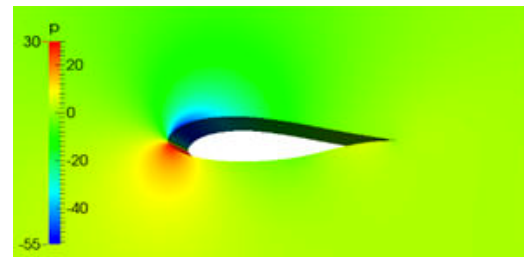

(a)
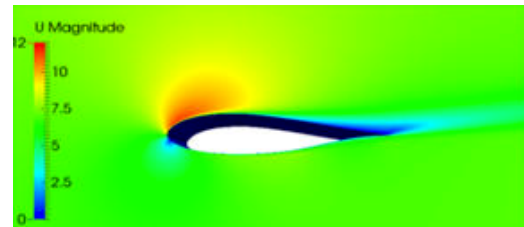
(b)

Figure 17 Wind speed average magnitude: (a) NACA0018 and (b) DU06W200 [Author]

(a)

(b)

Figure 18 Pressure distribution at airfoils (a) NACA0018 and (b) DU06W200 [Author]

This phenomenon produces turbulent flow quickly since the boundary layer cannot follow the pressure increase [3].

A consequence of the mentioned effects is quantified at the lift and drag coefficients presented in Table 12.

The DU06W200 produces 20% more lift coefficient than NACA0018, and its drag coefficient differs only by 6%. Therefore, the airfoil DU06W200 shows a better aerodynamic performance than the NACA0018 under the wind flow conditions of Chicamocha's River.

4. Conclusions

- Implementation of Vertical Axis Wind Turbines is feasible at Chicamocha's river, where average wind speed is 7 [m/s] and average wind power density is 485 [W/m^2].

- The "simpleFoam" solver is validated by using the Spalart-Allmaras fv3 turbulence model by its accurate results with a difference of 12% in comparison with experimental tests from literature.

- The airfoil NACA0018 shows its higher performance at an angle of attack of 10º where the lift and drag coefficients ratio has the greatest value: 10.3 approximately.

- The new airfoil DU06W200 presented these results:

    - Its lift coefficient increase 20% with the same drag loses as the NACA0018 airfoil at Chicamocha's river wind speed.

    - Lift coefficients for the DU06W200 airfoil at Reynolds numbers between 2×10^5 and 3.4×10^4, are 23% greater than the NACA0018 ones.

    - Therefore, the DU06W200 airfoil shows a better aerodynamic efficiency for vertical axis wind turbines' blades under wind properties of Chicamocha's canyon.

5. Future work

The wind energy potential at Chicamocha's canyon should include measurements during night time. In addition, the incidence of wingtip vortex on the finite wings should be calculated as well as the influence of the three airfoils distribution under unsteady simulations. Finally, the geometry of the troposkein shape for the total wing design should be compared with a straight blade design.

6. Acknowledgments

References

[1] *Colombia: tendencias a largo plazo del sector energía en Colombia*, Unidad de Planeación Minero Energética, Cartagena, Colombia, 2014.

[2] E. M. Villammizar, "Estudio sobre el impacto turístico y económico del parque nacional del chicamocha en el municipio de san gil," Ungraduathe thesis, Universidad Industrial de Santander, Santander, Colombia, 2007.

[3] M. C. Claessens, "The design and testing of airfoils for application in small vertical axis wind turbines," M.S. thesis, Delft University of Technology, Delft, Países Bajos, 2006.

[4] M. Raciti, G. Simioni, and E. Benini, "Numerical analysis of the influence of airfoil asymmetry on vawt performance," *International Journal of Mechanical, Aerospace, Industrial, Mechatronic and Manufacturing Engineering*, vol. 6, no. 1, pp. 75–84, 2012.

[5] S. Hsing, W. W. Liou, A. Shabbir, Z. Yang, and J. Zhu, "A new k-ɛ eddy viscosity model for high reynolds number turbulent flows," *Computers & Fluids*, vol. 24, no. 3, pp. 227–238, Mar. 1995.

[6] C. Monir, C. Abhishek, and G. Bharat, "Cfd analysis of horizontal axis wind turbine blade for optimum value of power," *International Journal of Energy Environment*, vol. 4, no. 5, pp. 825–834, 2013.

[7] M. S. H. Boutilier, "Experimental investigation of transition over a NACA 0018 airfoil at a low reynolds number," M.S. thesis, University of Waterloo, Ontario, Canada, 2011.

[8] G. Elhussien, A. Hassan, and M. Elsayed, "Numerical Investigation of medium range Re numbers Aerodynamics Characteristics for NACA0018 Airfoil," *CFD Lett.*, vol. 6, no. 4, pp. 175–187, Mar. 2014.

[9] K. Rogowski, M. O. Laver, and R. Maroński, "Steady and unsteady analysis of naca 0018 airfoil in vertical-axis wind turbine," *J. Theor. Appl. Mech.*, vol. 56, no. 1, pp. 203–212, 2018.

[10] P. M. Kumar, R. Kulkarni, N. Srikanth, and L. Teik, "Performance assessment of darrieus turbine with modified trailing edge airfoil for low wind speeds," *Smart Grid and Renewable Energy*, vol. 8, no. 12, pp. 425–439, Dec. 2017.

[11] S. Yarusevych and M. S. H. Boutilier, "Vortex shedding of an airfoil at low reynolds numbers," *AIAA Journal*, vol. 49, no. 10, pp. 2221–2227, 2011.

[12] P. Spalart and S. Allmaras, "A one-equation turbulence model for aerodynamic flows," presented at 30th Aerospace Sciences Meeting and Exhibit, Seattle, WA, 1992. [Online]. Available: https://arc.aiaa.org/doi/10.2514/6.1992-439

[13] Cañón del chicamocha. [Google Maps]. Accessed Feb. 15, 2019. [Online]. Available: google.com/maps/place/Cañón+del+Chicamocha/@6.8126222,-72.998592,8984m/data=!3m1!1e3!4m5!3m4!1s0x8e6976f20decd421:0x201ace7fe50af23c!8m2!3d6.815869!4d-72.9897054

[14] J. F. Manwell, J. G. McGowan, and A. L. Rogers, *Wind Energy Explained*, 2nd ed. Wiley, 2010.

[15] D. C. Wilcox, *Turbulence Modeling for CFD*. La cañada, California: DCW Industries, 1994.

[16] J. M. Fernández, *Técnicas numéricas en ingeniería de fluidos: Introducción a la dinámica computacional de fluidos (CFD) por medio del método de volúmenes finitos*, 1st ed. Barcelona, España: Editorial Reverté, 2012.

[17] K. HyeongKim, Y. Soo, and M. Senda, "Large eddy simulation of turbulent flow past a square cylinder confined in a channel," *Computers & Fluids*, vol. 3, no. 1, pp. 81–96, Jan. 2004.